Expected radiation environment and damage for YBCO tapes in compact fusion reactors

# Expected radiation environment and damage for YBCO tapes in compact fusion reactors

D. Torsello,[1,2,*] D. Gambino,[3,*] L. Gozzelino,[1,2] A. Trotta,[4] and F. Laviano[1,2]

[1] *Politecnico di Torino, Department of Applied Science and Technology, Torino 10129, Italy*
[2] *Istituto Nazionale di Fisica Nucleare, Sezione di Torino, Torino 10125, Italy*
[3] *Theoretical Physics Division, Department of Physics, Chemistry and Biology (IFM), Linköping University, SE-581 83 Linköping, Sweden*
[4] *Eni S.p.A.*

(Dated: September 19, 2022)

We investigate the neutron damage expected in the high temperature superconducting tapes that will be employed in compact fusion reactors. Monte Carlo simulations yield the expected neutron spectrum and fluence at the magnet position, from which the primary knock on atom energy distributions can be computed for each atomic species composing the superconductor. This information is then employed to characterize the displacement cascades, in terms of size and morphology, through Molecular Dynamics simulations. The expected radiation environment is then compared to the neutron spectrum and fluences achievable at the facilities currently available for experimental investigation, in order to highlight similarities and differences that could be relevant to the understanding of the radiation hardness of these materials in real fusion conditions. We find that the different neutron spectra result in different damage regimes, the irradiation temperature influences the amount of the generated defects, and the interaction of the neutrons with the superconductor results in a local increase of temperature. These observations suggest that further experimental investigations in different regimes are needed, and that some neutron shielding will be necessary in compact fusion reactors.

## I. INTRODUCTION

In recent years, compact nuclear fusion technology has risen a huge interest thanks to its disruptive potential for energy production with associated low environmental impact [1]. The key enabling technology for compact fusion is that of high-temperature superconducting (HTS) tapes, surprisingly not for their high critical temperature but for their high critical current at high field. As a matter of fact, only HTSs allow the production of magnets able to generate 20 T (and higher) fields with the size and stability requirements necessary for the development of fusion reactors [2].

Despite the great improvements in magnet technology and reactor design recently achieved, several challenges still need to be faced in order to deliver fusion reactors, one of the greatest being the evaluation and optimization of radiation hardness of the involved materials, including HTSs [3].

In the plasma, two neutron-producing fusion reactions will mainly take place, one between D and D, producing 2.45 MeV neutrons and one between D and T, producing 14.1 MeV neutrons. The latter is expected to be responsible for $\gtrsim$ 99% of all the generated neutrons [4], with a flux of the order of $2 \times 10^{20}$ n/s in ARC-like fusion power plant [5]. Within the compact tokamak concept physical space is intrinsically limited, therefore shielding will never be able to fully protect the Toroidal Field (TF) magnets without leading to technically infeasible designs. Thus, all TF magnets will experience some degree of radiation damage, making it a crucial topic that the community should deal with. Moreover, the combination of high energy and flux, also makes it impossible to test the materials at these exact radiation conditions with the facilities available as of today [6].

For this reason, all the research carried out on the radiation hardness of HTS tapes is either carried out with fission neutrons [7–13] or with ion irradiations [3, 14], yielding extremely valuable but unavoidably incomplete information. We suggest that a full understanding of radiation damage in HTS tapes can be achieved through the comprehensive analysis of several experimental approaches, each shedding light on specific issues, combined with a thorough computational investigation of the expected damage at the working conditions.

For this reason, here we investigate the expected damage on 2G HTS ($REBa_2Cu_3O_7$ - REBCO, where the rare earth could be Y, Gd, etc.) tapes at the working conditions in the ARC plant concept (considering the design proposed in Ref. [5]) for a compact fusion reactor by combined Monte Carlo (MC) and Molecular Dynamics (MD) simulations. This study yields the energy spectrum, fluence and flux of neutrons impinging on the magnet region, as well as the expected damage in the superconductor in terms of displacement per atom (dpa), transmutation yield, displacement cascade size, morphology and density. Finally, a comparison with the damage resulting from performed experiments at the main available irradiation facilities is carried out, allowing us to suggest additional experimental approaches. This multi-simulation approach ultimately aims to provide the understanding of the microstructural evolution of the REBCO under

* These two authors contributed equally

irradiation that is necessary to connect the fluence and spectra of neutrons to the HTS performance degradation.

## II. METHODS

### A. Monte Carlo simulations

The Monte Carlo code PHITS [15] was employed to simulate the transport and interaction of neutrons and secondary particles with a target designed to capture all the features of the ARC nuclear fusion reactor design relevant to the damage of REBCO tapes.

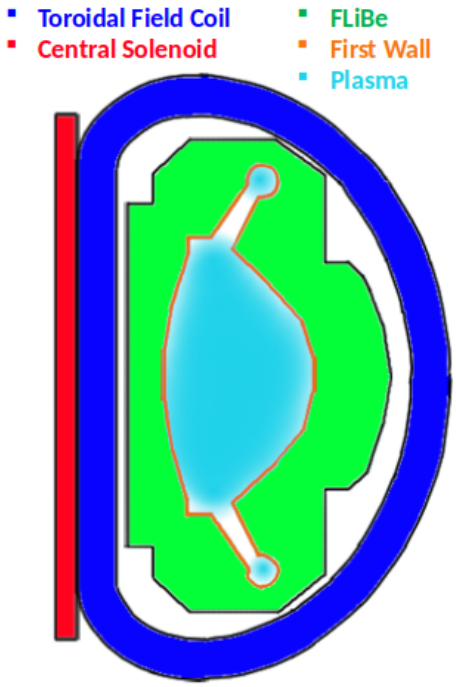


FIG. 1: Schematic view of the elements of the ARC nuclear fusion reactor design proposed in [5] that are relevant for the Monte Carlo simulations. The vacuum vessel, not shown, surrounds the FLiBe tank and is part of the layered first wall.

The region of interest for this study is the REBCO-tape TF magnet visible in blue in the scheme in Fig. 1 for the ARC design considered here [5]. The 14.1 MeV neutrons generated by the plasma interact with the First Wall (FW), the steel of the Vacuum Vessel (VV) and with the molten FLiBe salts before reaching the superconductor. PHITS allows investigating the amount and the energy spectrum of the neutrons that reach the HTS tapes. The most computationally efficient way to do so, is to consider a point-like, monochromatic (14.1 MeV), directional source impinging on a large multilayered slab consisting of a sequence of the materials placed between the plasma and the TF magnet with their respective thicknesses, as summarized in Table I. The last layer of the target, the YBCO, is the only one not to scale, and is made thicker to collect a larger statistics without increasing computational time. We choose YBCO as representative of REBCO because it has been widely studied and because an interaction potential for MD is already available and validated [16].

| Component | Material | Density ($g/cm^3$) | Thickness (cm) |
|---|---|---|---|
| FW | W | 19.25 | 0.1 |
| VV | Inconel steel | 8.44 | 1 |
| Molten Salt | $F_4Li_2Be$ | 1.94 | 2 |
| Multiplier | Be | 1.85 | 1 |
| VV | Inconel steel | 8.44 | 3 |
| Molten Salt | $F_4Li_2Be$ | 1.94 | 100 |
| VV | Inconel steel | 8.44 | 3 |
| TF | $YBa_2Cu_3O_7$ | 6.40 | 20 |

TABLE I: Details of the target design employed in the PHITS simulations, following Ref. [5].

The PHITS code (version 3.20) [15] was employed with the event-generator mode to compute the neutron energy spectrum impinging on YBCO (employing an energy-resolved T-Cross Tally), and the damage produced in it in terms of dpa and transmutation products (employing the T-dpa and T-Yield Tallies, respectively). The INCL [17] and Kurotama [18] models were selected for the simulations to compute nuclear reactions induced by neutrons and provide reaction cross sections of nucleon-nucleus and nucleus-nucleus. The simulations were run with a high enough statistics ($\gtrsim 10^6$ source particles) so that all the quantities of interest have an associated statistical uncertainty smaller than 5%. All results are normalized to the number of simulated neutrons, so that they can be scaled to obtain the expected values for a specific operation time. Moreover, in order to obtain fluences it is necessary to consider the geometry of confinement of the plasma. Considering an isotropic neutron emission, the toroidal geometry imposes a $1/r$ radial decrease of the fluence from the FW outwards, since the particles distribute approximately over the surface area of a torus. Despite the fact that the spectrum and fluences obtained here are in reasonable agreement with those from 3D simulations of a similar design [19], it is important to highlight that fine features of the spectra and fluences in different regions of the magnet system can only be captured with a full geometry implementation. Considering the spatial constraints in the design, a precise knowledge of the radiation damage over the magnet volume will be necessary to optimize the shielding design. However, at this stage it would represent an unnecessary complexity and we will implement this refinement in later studies.

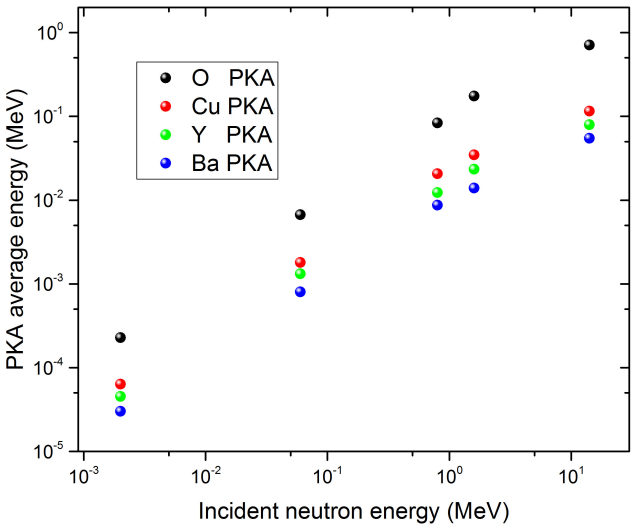


FIG. 2: Log-log plot of the average energy of the PKA as a function of the impinging neutron energy for all atomic species in YBCO.

### B. PKA energy calculation

Once the neutron energy spectrum is known, it is necessary to obtain information about the Primary Knock-on Atom (PKA) that starts the damage cascade in order to perform MD simulations to investigate its morphology [16]. To achieve this result the code SPECTRA-PKA was employed: it takes into account the composition of the target, the incident neutron spectrum and nuclear recoil cross-section matrices to yield elemental PKA spectra and distributions [20].
From the PKA distributions of each atomic species, one can choose to consider the average PKA energy as roughly representing the initiation of the cascade for MD simulations. This average PKA energy approximately follows a power law dependence on the incident neutron energy, as shown in Fig. 2 for the case of PKAs resulting from monochromatic neutron beams.

### C. Molecular Dynamics

MD simulations were carried out to study the size and morphology of displacement cascades for different PKA energies and irradiation temperatures chosen to emulate the ARC case and various experimental irradiation conditions. Interatomic interactions in YBCO were described with the potential developed in Ref. [16], which consists of a combination of Buckingham [21] and Coulomb potential splined to the universal Ziegler–Biersack–Littmark potential [22] at short distances, where this last interaction is included to account for the strong nuclear repulsion at small interatomic distances often occurring during displacement cascades. This potential was shown [16] to give satisfactory agreement with *ab initio* results.

For each set of conditions (type of PKA, initial kinetic energy of the PKA, and temperature), we carried out 11 simulations with different initial directions of the PKA velocity. The configurations were previously thermalized in the NPT ensemble as to ensure statistical independence of the initial conditions of the displacement cascades. Three cascades were initiated with the velocity in the c-direction (most likely condition for common experimental geometries), whereas for the last eight the direction of the velocity was picked randomly.

Following the methodology described in [16] for the simulation of displacement cascades, we rescaled the velocity of a single atom to represent the kinetic energy transferred from the neutron to the PKA, and then allowed the system to evolve in response to this stimulus. For these simulations, we defined a spherical region within which the dynamics is evolved in the NVE microcanonical ensemble. In order to disperse the excess energy and maintain the system at the target temperature, we applied a velocity-rescaling thermostat to the atoms outside the sphere. The diameter of the sphere was taken as 90% of the shortest edge of the supercell. The size of supercells considered in the MD simulations was large enough as to avoid that either the PKA atom or the displacement cascade would reach the boundary of the sphere, and therefore avoid spurious effects due to the thermostat that could be introduced in the dynamics and the formation of defects. The simulations were carried out in two stages: in the first stage, representing the ballistic phase, the equation of motion were integrated with a timestep of $10^{-5}$ ps for the initial 2 ps to avoid too large atomic displacements that could disrupt the dynamics; in the second stage, the recombination phase, we employed a timestep of $10^{-3}$ ps and carried out the simulations for 100 ps, as to ensure a converged number of defects in the simulation.

## III. RESULTS AND DISCUSSION

### A. Neutrons impinging on the HTS tapes

The energy spectrum of neutrons reaching the TF magnet in the ARC design, calculated by MC simulations, is presented in Fig. 3 (together with the spectrum of the most employed experimental facility for neutron irradiation, the TRIGA reactor in Wien). In addition to the 14.1 MeV neutrons, a very broad distribution of neutron is present at lower energies. The jagged profile is due to the several materials crossed and nuclear reaction channels contributing to the neutron energy loss. Taking into account the expected neutron flux generated by the plasma ($2.2 \times 10^{20}$ n/s [5]) and the size of the ARC tokamak (torus of radii 1.85 m and 1.67 m), it is possible to estimate the resulting neutrons flux and fluence after 10 years of operation on the TF magnet for 14.1 MeV neu-

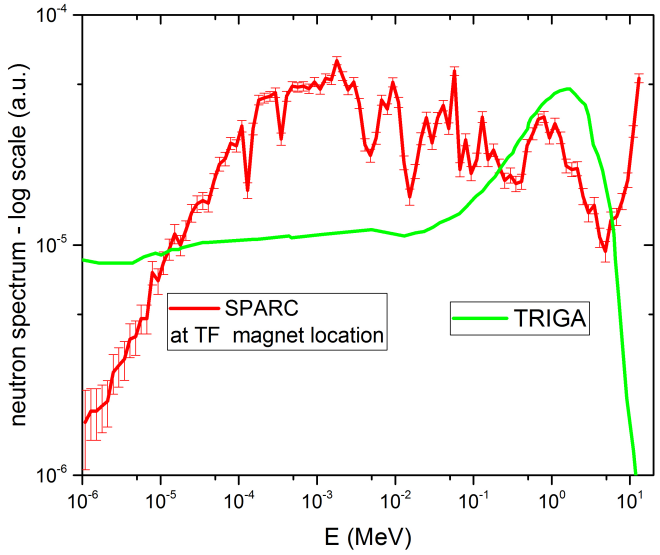


FIG. 3: Neutron spectrum impinging on the YBCO TF magnet (red line) compared to the TRIGA spectrum [23] (green) employed for most HTS tape neutron irradiation experiments.

trons and integrated fast neutrons (defined as neutrons with energy $> 0.1$ MeV [12]). These parameters, useful to guide future experimental investigations of HTS tapes radiation hardness, are summarized in Table II.

| Parameter | 14.1 MeV neutrons | Fast neutrons |
|---|---|---|
| Flux (n/(s m$^2$) ) | $9.6\times10^{13}$ | $5.1\times10^{14}$ |
| 10 years Fluence (n/cm$^2$) | $3.0\times10^{18}$ | $1.6\times10^{19}$ |

TABLE II: Expected radiation environment in ARC TF magnet.

### B. Expected damage

The MC simulations directly yield the expected damage in the ARC TF magnet in terms of dpa and transmutation products (summarized in Table III), while the details of the damage cascades need to be computed through PKA-SPECTRA and MD simulations.
The expected dpa in 10 years is 0.52, an extremely high value for a crystalline ceramic material with functional purposes.
The PKA distributions for each element in YBCO obtained for the ARC (at TF location) and TRIGA spectra are shown in Fig. 4. For the same neutron spectrum, the Ba and Y PKA have similar distributions due to their quite similar mass and abundance. For the same reasons, more Cu and O PKAs form, also peaking at higher energies.

From MD, details of the damage cascades can be estimated for each PKA species and energy, working temperature and as a function of time. This allows investigating recombination effects, local temperature increase under beam exposure and the morphology of cascades, that strongly affects pinning properties. The time evolution of the number of defects is shown in Fig. 5 for some illustrative energy-species combinations: up to 50% of the produced defects recombine in less than 5 ps even at cryogenic temperatures (clearly visible from the inset). After the recombination phase, the number of defects is stable on the time scales that can be explored with MD, hence the situation obtained at the end of the simulations provides a good description of the system also after longer times such as those experimentally accessible.

An example of the damaged region after the recombination period is given in Fig. 6 for the case of a 7 keV Ba PKA at T=20 K (top panel) and for a 110 keV Ba PKA at T=300 K (bottom panel). As visible from Fig. 4, the lower energy is typical both for the ARC TF and for the experiments carried out at TRIGA, while the higher one is mostly relevant for ARC conditions. The size and branching of the cascades greatly changes with energy, possibly having an impact on pinning and therefore on the critical current at high field of irradiated tapes. Table IV summarizes the volume of the cascades and the average number of defects at different energies

| Parameter | ARC (expected in 10 years) | TRIGA (Fischer et al. [12]) |
|---|---|---|
| Fast neutron fluence (n/cm$^2$) | $1.6\times10^{19}$ | $4.0\times10^{18}$ |
| dpa | 0.52 | 0.02 |
| H yield (appm/dpa) | 0.5 | 0 |
| He yield (appm/dpa) | 10.6 | 0 |

TABLE III: Expected neutron damage in ARC TF magnet compared to that calculated for the highest neutron fluence reported in literature [12].

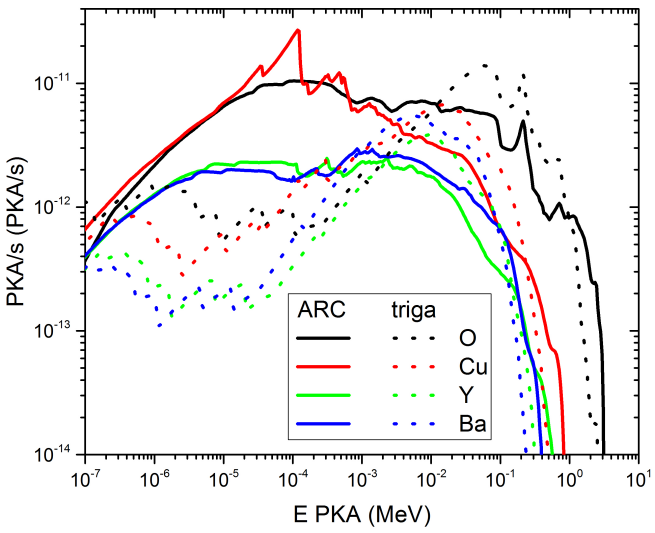


FIG. 4: PKA distributions for each element in YBCO obtained for the ARC (at TF location, solid lines) and TRIGA spectra [23] (dotted lines).

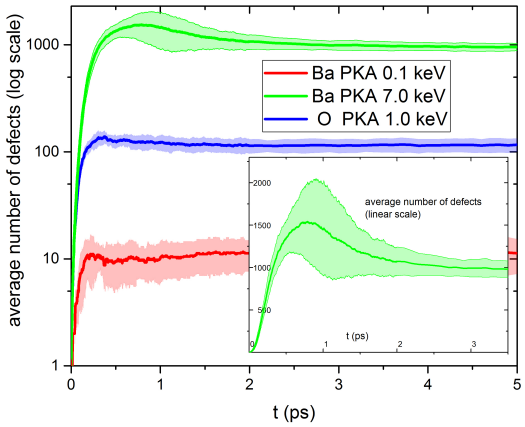


FIG. 5: Time evolution of the number of defects following from the collision of a PKA (Ba with E = 0.1 keV in red, O with E = 1.0 keV in blue and Ba with E = 7.0 keV in green) with a neutron at T = 20 K. 11 simulations were performed for each case, the lines represent the average values and the shaded areas the standard deviations. The data in the main panel is shown in log scale, linear scale is used in the inset to show the recombination peak.

| PKA | T (K) | $E_{PKA}$ (keV) | $\langle V \rangle$ (nm$^3$) | $\langle N_{def} \rangle$ |
|---|---|---|---|---|
| Ba | 20 | 0.1 | $0.04 \pm 0.04$ | $11 \pm 4$ |
| O | 20 | 1 | $1.3 \pm 0.7$ | $115 \pm 17$ |
| Ba | 20 | 7 | $17.6 \pm 4.5$ | $936 \pm 70$ |
| Ba | 20 | 110 | 185.6 | 12472 |
| Ba | 300 | 0.1 | $0.06 \pm 0.03$ | $17 \pm 3$ |
| O | 300 | 1 | $1.6 \pm 0.4$ | $149 \pm 10$ |
| Ba | 300 | 7 | $19.8 \pm 7.1$ | $1205 \pm 72$ |
| Ba | 300 | 110 | 308.9 | 19092 |

TABLE IV: Volume of defective region and number of defects from MD for different PKA, temperatures and PKA energies, corresponding to volume inside the green mesh of Fig. 6.

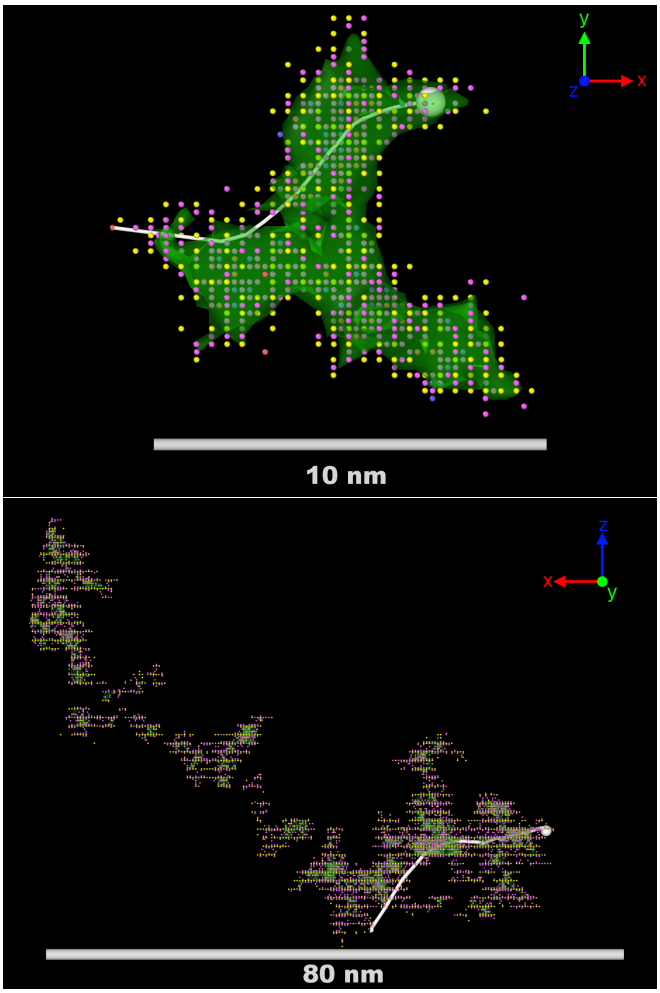


FIG. 6: Projections of the damage cascade resulting from MD simulations of a 7 keV Ba PKA at T=20 K (top) and of a 110 keV Ba PKA at T=300 K (bottom) at the end of the ballistic period. Colored spheres represent vacancies and interstitial defects in different lattice sites (Ba in red, Y in violet, Cu in yellow and O in magenta), whereas the large white sphere and its "tail" represent the Ba PKA. The green mesh identifies the amorphized region.

and temperatures. The dependence of the number of defects in a cascade on PKA energy is shown in Fig. 7 for all conditions simulated in the present work. Here one can see that the PKA species has a negligible impact on the number of defects, whereas a higher temperature induces a steeper increase of the number of defects with increasing PKA energy.

Since in experiments often the particles are hitting the samples in the c-direction [24], it would be interesting to compare the average number of defects produced by cascades initiated in the c-direction with the average number of defects from all cascades. From the present investigation, there seems to be a small difference in temperature behavior between the average number of defects produced by cascades initiated in the c-direction as compared to all directions, which could entail that different thermally activated diffusion mechanisms could come into play and favor different directions at different temperatures. However, the difference is not statistically relevant, and since the averages are based on small numbers of configurations and only two temperatures, further investigation is needed to check this temperature behavior.

MD simulations highlighted another interesting aspect: following the collision, the temperature averaged over the active simulation area (a sphere of radius 10-100 nm depending on the simulation) increases abruptly, and an increase up to about 1.3 K persists even after

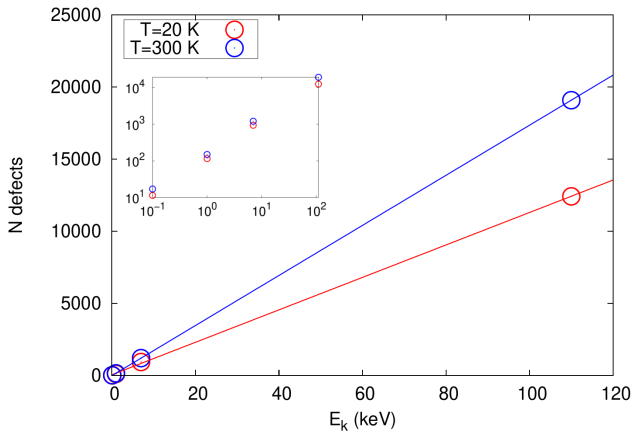


FIG. 7: Final number of defects as a function of PKA initial energy at 20 and 300 K. The lines are linear fits to the results that highlight the change of slope. The inset shows the same data in log-log scale.

100 ps (see Fig.8). Such an effect might be relevant for the current transport performance of HTS tapes under high flux irradiation: the critical current could be locally depressed, and such hot spots might promote instabilities [25, 26]. However, in the simulations heat is dissipated through the thermostat applied at the boundary of the cell, therefore the absolute changes of temperature could be affected by artifacts, and its maximum value is of course dependent on the size of the active simulation area.

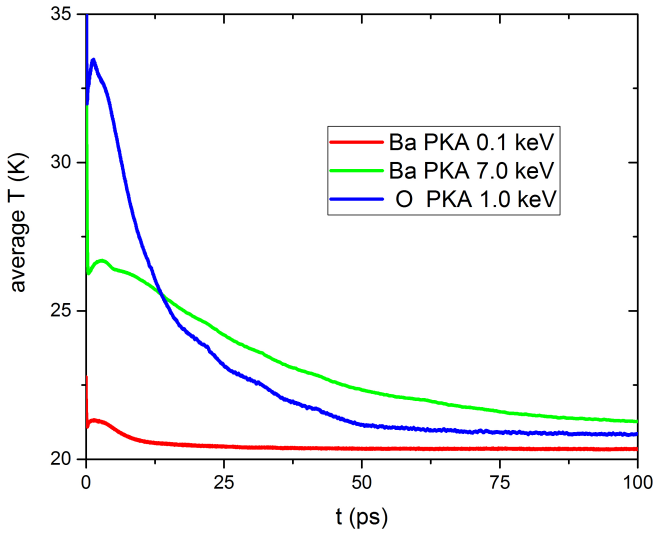


FIG. 8: Time evolution of the average temperature of the simulation region following from the collision of a PKA with a neutron.

### C. Comparison with experiments

The spectrum from the TRIGA fission reactor in Wien [23] is compared in Fig. 3 to the one expected at the TF in the ARC design. The main feature is a fast neutron peak centered at 1.7 MeV, to be compared with the 14.1 MeV peak and the broad low energy feature representative of the ARC spectrum.
Comparing PKA spectra for the ARC and TRIGA cases (Fig. 4), some differences arise: the broader neutron distribution expected at the TF magnet position in ARC results in much broader PKA distributions, with high production rates over several orders of magnitude. On the other hand, in TRIGA, the PKAs are mostly generated by the 1.7 MeV neutron peak, yielding narrower PKA distributions.
The size of the cascade shown in the upper panel of Fig. 6, produced by a 7 keV Ba PKA (typical PKA for TRIGA experiments) is comparable to that reported by Linden *et al.* [27] after TEM observation.
The maximum fast neutron fluences reported for irradiation experiments at TRIGA are of the order of $4\times10^{18}$ n/cm$^2$, corresponding to the integrated fast neutron fluence expected in ARC over a period of about 2.5 years. At this fluence the critical temperature of HTS tapes was found to decrease by about 12 %, while the critical current of the worst performing tape at 30 K and 15 T was reduced to 50% of its pristine value. However, the fast neutron fluence alone is not representative of the radiation environment. In fact the corresponding dpa from such TRIGA experiments, calculated by PHITS, is about $2\times10^{-2}$, 26 times smaller than the expected damage in ARC. This result, combined with an extrapolation of the experimental $T_c$ data, strongly suggests that some neutron shielding design will be necessary in compact fusion reactors. However, further experimental investigations are needed to better investigate the expected damage regime, the impact of cryogenic environment and of *operando* conditions (presence of a high transport current and dc magnetic field) on the superconducting properties modifications.

## IV. CONCLUSIONS

In summary, we presented a multiscale modelling approach for the evaluation of neutron damage in HTS magnet materials for compact fusion reactors, in which Monte Carlo and Molecular Dynamics simulations are sequentially employed to investigate the radiation environment that will be experienced by the magnets and the resulting damage in the superconductor. The analysis for the ARC design, combined to literature data of neutron induced superconducting properties modifications, indicates that neutron shielding will be necessary to protect the TF magnet. Moreover, MD simulations suggest that local heating in the cascade region might last long enough to

have a non negligible effect on the HTS performance. Overall, the broad neutron spectrum and high fluence expected at the TF position in ARC, the dependence of the cascade size on PKA energy and working temperature, and the extreme *operando* conditions, suggest that further experimental works are needed to investigate the impact of all these aspects on the performance of HTS under neutron irradiation.

## ACKNOWLEDGMENTS

All the authors are extremely thankful to Z Hartwig and D Fischer for fruitful discussion. DT, LG and FL acknowledge the support by the Italian Ministry of Education, University, and Research through Project PRIN HIBiSCUS, Grant No. 201785KWLE. DT also acknowledges the support by the "Programma Operativo Nazionale (PON) Ricerca e Innovazione 2014–2020". DG is very thankful to Samuel Murphy for sharing the interatomic potential and for useful discussions. The molecular dynamics simulations were enabled by resources provided by the Swedish National Infrastructure for Computing (SNIC), partially funded by the Swedish Research Council through grant agreement no. 2018-05973.

[1] N. M. Strickland, Superconductor Science and Technology **34**, 110502 (2021).
[2] B. Sorbom, J. Ball, T. Palmer, F. Mangiarotti, J. Sierchio, P. Bonoli, C. Kasten, D. Sutherland, H. Barnard, C. Haakonsen, J. Goh, C. Sung, and D. Whyte, Fusion Engineering and Design **100**, 378 (2015).
[3] W. Iliffe, N. Peng, G. Brittles, R. Bateman, R. Webb, C. Grovenor, and S. Speller, Superconductor Science and Technology **34**, 09LT01 (2021).
[4] R. Tinguely, A. Rosenthal, R. Simpson, S. Ballinger, A. Creely, S. Frank, A. Kuang, B. Linehan, W. McCarthy, L. Milanese, K. Montes, T. Mouratidis, J. Picard, P. Rodriguez-Fernandez, A. Sandberg, F. Sciortino, E. Tolman, M. Zhou, B. Sorbom, Z. Hartwig, and A. White, Fusion Engineering and Design **143**, 212 (2019).
[5] A. Kuang, N. Cao, A. Creely, C. Dennett, J. Hecla, B. LaBombard, R. Tinguely, E. Tolman, H. Hoffman, M. Major, J. Ruiz Ruiz, D. Brunner, P. Grover, C. Laughman, B. Sorbom, and D. Whyte, Fusion Engineering and Design **137**, 221 (2018).
[6] J. Knaster, A. Moeslang, and T. Muroga, Nature Physics **12**, 424 (2016).
[7] R. Fuger, M. Eisterer, and H. W. Weber, IEEE Transactions on Applied Superconductivity **19**, 1532 (2009).
[8] M. Eisterer, R. Fuger, M. Chudy, F. Hengstberger, and H. Weber, Superconductor Science and Technology **23**, 014009 (2009).
[9] M. Chudy, R. Fuger, M. Eisterer, and H. W. Weber, IEEE Transactions on Applied Superconductivity **21**, 3162 (2011).
[10] R. Prokopec, D. Fischer, H. Weber, and M. Eisterer, Superconductor Science and Technology **28**, 014005 (2014).
[11] M. Jirsa, M. Rameš, I. Ďuran, T. Melíšek, P. Kováč, and L. Viererbl, Superconductor Science and Technology **30**, 045010 (2017).
[12] D. X. Fischer, R. Prokopec, J. Emhofer, and M. Eisterer, Superconductor Science and Technology **31**, 044006 (2018).
[13] R. Unterrainer, D. X. Fischer, A. Lorenz, and M. Eisterer, Superconductor Science and Technology **35**, 04LT01 (2022).
[14] K. J. Leonard, T. Aytug, A. A. Gapud, F. A. L. III, N. T. Greenwood, Y. Zhang, A. G. Perez-Bergquist, and W. J. Weber, Fusion Science and Technology **66**, 57 (2014).
[15] T. Sato, K. Niita, N. Matsuda, S. Hashimoto, Y. Iwamoto, S. Noda, T. Ogawa, H. Iwase, H. Nakashima, T. Fukahori, K. Okumura, T. Kai, S. Chiba, T. Furuta, and L. Sihver, Journal of Nuclear Science and Technology **50**, 913 (2013).
[16] R. Gray, M. J. Rushton, and S. T. Murphy, Superconductor Science and Technology (2022), https://doi.org/10.1088/1361-6668/ac47dc.
[17] A. Boudard, J. Cugnon, J.-C. David, S. Leray, and D. Mancusi, Phys. Rev. C **87**, 014606 (2013).
[18] K. Iida, A. Kohama, and K. Oyamatsu, Journal of the Physical Society of Japan **76**, 044201 (2007).
[19] J. W. Bae, E. Peterson, and J. Shimwell, Nuclear Fusion **62**, 066016 (2022).
[20] M. Gilbert, J. Marian, and J.-C. Sublet, Journal of Nuclear Materials **467**, 121 (2015).
[21] R. A. Buckingham and J. E. Lennard-Jones, Proceedings of the Royal Society of London. Series A. Mathematical and Physical Sciences **168**, 264 (1938).
[22] J. F. Ziegler and J. P. Biersack, in *Treatise on Heavy-Ion Science* (Springer, 1985) pp. 93–129.
[23] H. Weber, H. Böck, E. Unfried, and L. Greenwood, Journal of Nuclear Materials **137**, 236 (1986).
[24] T. Aoki, H. Ueda, A. Ishiyama, N. Miyahara, N. Kashima, and S. Nagaya, IEEE Transactions on Applied Superconductivity **21**, 3200 (2011).
[25] L. Li, L. Jiang, Y.-H. Zhou, A. V. Silhanek, and C. Xue, Superconductor Science and Technology **35**, 085002 (2022).
[26] F. Laviano, "Vortex avalanches in superconductors visualized by magneto-optical imaging," in *Vortices and Nanostructured Superconductors*, edited by A. Crisan (Springer International Publishing, Cham, 2017) pp. 133–157.
[27] Y. Linden, W. Iliffe, G. He, M. Danaie, D. Fischer, M. Eisterer, S. Speller, and C. Grovenor, Journal of Microscopy **286**, 3 (2022).